https://doi.org/10.1016/j.rcim.2018.07.012

Process parameters tuning and online re-slicing for robotized Additive Manufacturing of big plastic objects

Lara Rebaioli[1], Paolo Magnoni[1], Irene Fassi[1], Nicola Pedrocchi[1], Lorenzo Molinari Tosatti[1]

[1]*Consiglio Nazionale delle Ricerche, Institute of Industrial Technologies and Automation, via A. Corti 12, 20133 Milan, Italy*

* corresponding author: lara.rebaioli@itia.cnr.it

Abstract

Complex parts can be successfully manufactured by means of Additive Manufacturing (AM) techniques based on thermoplastic polymer extrusion, whose use for mass production is restricted by their slow printing speed. To address this limitation, a flexible AM platform for big plastic objects has been realized mounting an industrial screw-based extruder on an anthropomorphic robot. An experimental campaign has been performed to set a suitable range of relevant process parameters, with the aim of ensuring a regular deposited layer geometry. Moreover, a closed-loop control strategy has been developed to correct the robot height based on data measured during the material deposition, thus further improving the process parameter setting and compensating the material shrinkage or other unexpected defects. Eventually, an online re-slicing algorithm has been implemented to preserve the desired height of the manufactured object, despite the layer height changes. The proposed approach allows a deposition flow rate up to 1250 cm^3/h within a building volume limited only by the robot workspace.

Keywords: Additive Manufacturing, Rapid Prototyping, Anthropomorphic Robot, Performance Evaluation, Re-slicing

Nomenclature

e_k	Error between $\Delta x_{ref,k}$ and $\Delta \tilde{x}_{mean,k}$
v_t	Robot translation speed
$z_{reslice}$	z-coordinate in correspondence of which a re-slicing is ordered
w_{mean}	Measured mean layer width
β	Overlap factor
$\Delta x_{ref,k}$	Nominal layer height (k^{th} layer) with an additional height to guarantee an overlap between layers
$\Delta \tilde{x}_{mean,k}$	Measured mean layer height (k^{th} layer) with an additional height to guarantee an overlap between layers
Δz_{diff}	Difference between nominal and measured mean layer height
Δz_{mean}	Measured mean layer height

$\Delta z_{ref,k}$ Nominal layer height (k^{th} layer)

λ Proportional gain in the control law

ω_m Extruder motor rotational speed

1. Introduction and objectives

In recent years, Additive Manufacturing (AM) techniques based on the extrusion of thermoplastic polymers, such as Fused Deposition Modeling (FDM), have become widely used [1,2]. The AM processes allow the fabrication of customized and complex parts, but standard AM systems have a slow printing speed limiting their use for mass production. Consequently, the key targets for future manufacturing systems are a productivity improvement and an increment of achievable part size [3]. Industrial microextruders achieve a fused material deposition rate equal to 3 kg/hour, that is 10 to 20 times higher than the average deposition rate of commercial FDM systems [4,5]. Moreover, AM systems based on robotic platforms provide more flexibility, better motion software support and an industrial level of reliability, being able to replace FDM printers in some applications [6]. Eventually, using plastic pellets instead of commercial filaments allows a cost reduction and a higher freedom in material selection. Despite of these advantages, the additive manufacturing of big parts with high deposition rates has some limitations, e.g. non-optimally tuned process parameters could result in an irregular shape of deposited material and, then, in geometrical errors on the printed object. The material shrinkage during the cooling phase is another critical issue, since it could modify the deposited layer geometry. Moreover, the mismatch between the nominal geometry and the actual one is of utmost importance when the component is supposed to be assembled, as well as when the component need supports that have been designed according to the nominal geometry.

In this study, a flexible platform for the additive manufacturing of big objects has been realized modifying an industrial screw-based extruder and mounting it on an anthropomorphic robot and suitable methods have been designed to overcome the aforementioned drawbacks. This work proposes a procedure to set optimal values for the most important process parameters (i.e. rotational speed of the extruder motor, robot translation speed, nominal layer height commanded to the robot) (Section 3). This objective has been achieved thanks to a suitable experimental campaign on single-layer rectilinear tracks, which has been developed according to Design of Experiments (DoE). The described approach can be applied to different materials, as proved by the use of two polymeric materials in the reported experiments. This paper proposes also a closed-loop control strategy to correct the robot height when depositing many layers (Section 4.1). This procedure is based on a discrete control law and on the integration of sensors into the robotic system to make measurements during the material deposition. The sensor-guided corrections change the adopted layer height, hence this work implemented a fast online re-slicing algorithm to respect the desired dimension of the part, but requiring low computational times (Section 4.2). A representative case study of additive manufacturing of big parts, i.e. a piece of furniture, demonstrates the effectiveness of the proposed procedures (Section 5).

1.1. State-of-the-art

Only few examples of AM systems for plastic parts with deposition rates more than 20 times higher than standard high-end 3D printers (the so-called Big Area Additive Manufacturing – BAAM systems) can be found in literature. A system with a 15000 cm^3/h flow rate has been developed by the Oak-Ridge-National-Laboratory in collaboration with Cincinnati Inc. [7]. The final quality of the workpiece is affected by warpage, shrinkage and irregularities in the shape of the deposited layers. To limit this issues, a mechanical compactor could be included in the extruder design [5]. Moreover, materials with low warpage/shrinkage ratios (i.e. carbon fiber composites) can be used [5]. In this system the extruder has been mounted on a gantry-style robotic cell, but there are some commercial setups in which robotized AM systems have been created using anthropomorphic robots [8,9]. A further example in the market is the Deltawasp 3MT [10], a 3 degrees-of-freedom parallel kinematic machine equipped with an extrusion head on the mobile platform. This machine achieves a high flow rate through a feeding system that supplies pellets to the extrusion head. However, a limited layer resolution is achievable, as well as there are difficulties in a proper control of the deposition [11]. Nevertheless, two issues are still poorly investigated. Firstly, there is still lack of discussion about the procedure to find printing parameters or control loops to apply during the deposition process. Secondly, the path-planning and slicing issues regarding such machines are still not sufficiently addressed.

Focusing on the former issue, the existing literature dealing with the estimation of optimal deposition parameters considers only standard 3D printing, and not BAAM. Sood [12] studied the influence of process parameters (namely, layer thickness, orientation, raster angle, raster width and air gap), which can affect the dimensional accuracy, the surface roughness and the mechanical properties of the printed part. The work by Sood is based on the assumptions that each deposited layer has a regular geometry, as typical of many studies [13-15]. However, when using a large deposition rate or non-standard materials, this assumption cannot be considered true; therefore, this study will focus on setting the fundamental parameter values to guarantee a regular deposition of each layer.

Many works are available in literature about the monitoring of laser-based metal AM processes to achieve a better deposition and Mazumder et al. [16] resume the state-of-art. Fewer works are focused on the process monitoring in case of plastic deposition techniques. The temperature of the deposited material have been measured in the works by Dinwiddie et al. [17,18], while Faes et al. [19] integrated a laser triangulation scanner into a standard 3D printer to acquire the shape of the deposited material. However, most FDM machines are not equipped with any feedback system. The possible causes of this lack are: (i) a feedback control is not required thanks to the FDM process stability for standard deposition rates (i.e. for standard nozzle diameter values); (ii) control loops are more difficult to implement in 3D printers and CNC machines than in robot controllers where multi-threading can be exploited; (iii) the standard AM systems have a relatively low cost.

Focusing on the latter issue, the computational time required to generate the tool path is very large according to the industrial practice. Indeed, CAM software are designed for the slicing of small parts and create paths with a large amount of points at a small

distance. According to Minetto et al. [20], the algorithms for the path generation for a 3D printer starting from a 3D triangle mesh can be divided in three phases (Fig. 1): (i) the "slicing step", where the geometric model is intersected with parallel planes to obtain the contour of each material layer; (ii) the "contour construction step", where the segments produced by slicing are organized into one or more closed polygons that delimit the object; (iii) the "connection step", where the contours are connected to create the printing path. Some strategies to improve each step of the layered manufacturing path planning can be found in [21-25].

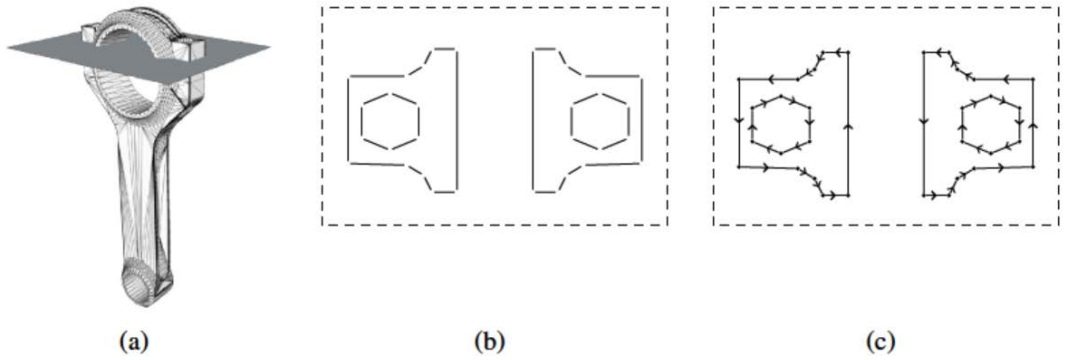

Fig. 1 *Steps in the additive layered manufacturing process planning: (a) slicing step; (b) contour construction step; (c) path creation step (adapted from [20]).*

The most critical phase for the computational time is the slicing step. As an example, the first algorithms used to slice a STL file for stereolithographic applications employed more than 60% of the time to prepare the part to be produced [26]. These algorithms were highly inefficient, because they tested every cutting plane against every triangle. Over the years, the computational time required by the slicing step has been reduced thanks to the sorting of triangles in sub-groups to avoid useless intersection checks [27] and to parallel computing [26]. This latter method has been applied also in this work.

2. Setup description

The developed BAAM robotic system is composed by a 6-axes ABB IRB-2600 anthropomorphic robot (20 kg of payload, 1.65 m of reachability) equipped with a single screw industrial extruder by Gimac. The extruder belongs to the "microextruders" family of Gimac products and has these features: a pellet feeding system (hopper), four heated zones and a conic deposition nozzle (with a Ø 2 mm hole) [4]. The extrusion head is equipped with an Omron laser triangulation sensor (Fig. 2b) to measure distances within the measurement range of 50 mm ± 10 mm and a resolution up to 2 µm. An 80 x 80 mm heated bed can guarantee an adequate adhesion with many different materials. The robot controller communicates via TCP/IP with the computer where the slicing software and the online re-slicing software run. The computer is a Lenovo Y700, with 6th generation I7 CPU, 2.6 GHz and a NVIDIA GeForce GTX950M graphic card compatible with 9.1 CUDA (Compute Unified Device Architecture) libraries [28].

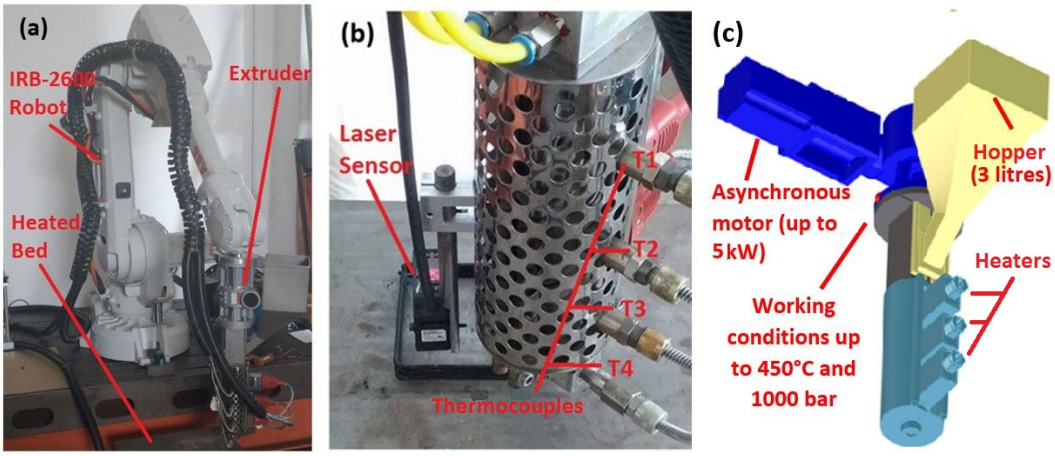

Fig. 2 *(a) robotic system to print big parts with plastic materials, developed by ITIA-CNR with the collaboration of Gimac S.r.l.; (b) laser measurement sensor attached to the extrusion head; (c) scheme of the extruder.*

3. Process parameter tuning

3.1. Objectives and definitions

The process parameter tuning phase aims at finding optimal values for relevant process parameters (namely, extruder motor rotational speed, robot translation speed, nominal layer height), which are the values ensuring a regular and constant geometry of the deposited layer. A suitable experimental campaign was developed according to Design of Experiments (DoE) [29] to achieve this goal and to point out the relationship between the process parameters and the deposited track geometry.

The two most common materials used in conventional FDM are the polylactid acid (PLA), being easy to print thanks to its low melting point, and the acrylonitrile butadiene styrene (ABS), which has higher flexibility, strength and heat-resistance than PLA. For this reason, PLA (NatureWorks Ingeo™ Biopolymer 4043D) and ABS (Eni Versalis Sinkral® B432/E) were selected as the target materials of the whole experimental work. Pure PLA is transparent and would not be visible by the laser measurement sensor (Fig. 2b), thus a specific black colorant additive was combined with PLA directly in the extruder hopper.

Tab. 1 *Constant parameters for track deposition experiments.*

Factor	Value	
	PLA	ABS
Track length (mm)	200	300
Number of layers	1	1
Temperature – extruder zone 1 [T_1] (°C)	156	220
Temperature – extruder zone 2 [T_2] (°C)	164	230
Temperature – extruder zone 3 [T_3] (°C)	155	220
Temperature – extruder zone 4 [T_4] (°C)	147	210
Temperature – heated bed (°C)	88	120

The experimental campaign of the process parameter tuning phase was performed considering the simplest possible geometry, which consists of single-layer rectilinear tracks that were deposited with the constant parameters of

Tab. **1**. The temperatures of the four heating zones (Fig. 2b) were selected based on preliminary experiments as the temperatures allowing both a satisfying deposition and a quick solidification of the material.

After printing, the tracks were allowed to cool and, subsequently, their height and width were measured by a micrometer caliper in five equally-spaced positions within each specimen.

3.2. Experimental design

Tab. **2** summarizes the full factorial experimental designs that were specifically studied to evaluate the effects of the three selected process parameters (extruder motor rotational speed, robot translation speed, nominal layer height) on the deposited layer geometry for both PLA and ABS. Each factor has three levels, whose values were determined based on preliminary experimental campaigns, and in total there are $3^3 = 27$ different experimental conditions. Both experimental designs consisted of 81 completely randomized runs, since three replicates were performed for each experimental condition.

Tab. 2 *Experimental designs.*

Factor	**Symbol**	**Levels**	
		PLA	**ABS**
Extruder motor rotational speed (rpm)	ω_{m}	400, 650, 900	400, 650, 900
Robot translation speed (mm/s)	v_{t}	15, 20, 25	15, 20, 25
Nominal layer height (mm)	Δz_{ref}	1.5, 2, 2.5	1, 1.5,

The selected experimental responses are the difference between the nominal and actual layer height (Δz_{diff}) and the mean track width (w_{mean}). The mean height (Δz_{mean}) and width (w_{mean}) of each track are calculated as the average of the five measured values, then Δz_{diff} is obtained as follows:

$$\Delta z_{diff} = \Delta z_{ref} - \Delta z_{mean} \tag{1}$$

3.3. Experimental results

Fig. 3 *Examples of PLA deposited tracks at the experimental conditions A: ω_m = 650 rpm, v_t = 20 mm/s, Δz_{ref} = 2.0 mm; B: ω_m = 900 rpm, v_t = 15 mm/s, Δz_{ref} = 1.5 mm; C: ω_m = 400 rpm, v_t = 25 mm/s, Δz_{ref} = 2.5 mm.*

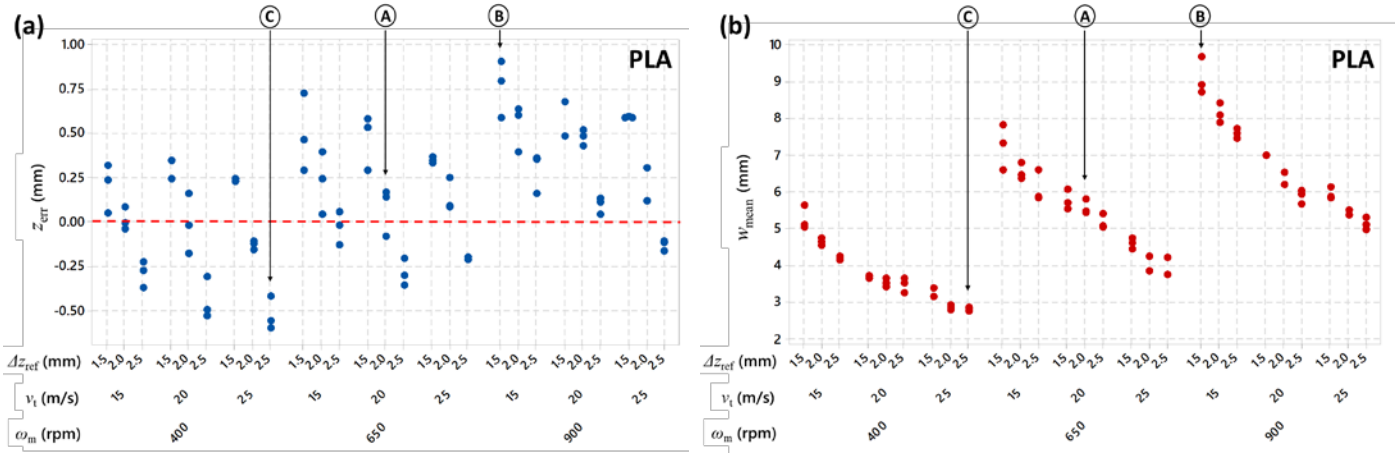

Fig. 4 *Experimental results for PLA: (a) individual value plot of mean height difference (Δz_{diff}); (b) individual value plot of mean width (w_{mean}) [A, B and C refer to the experimental conditions listed in Fig. 3].*

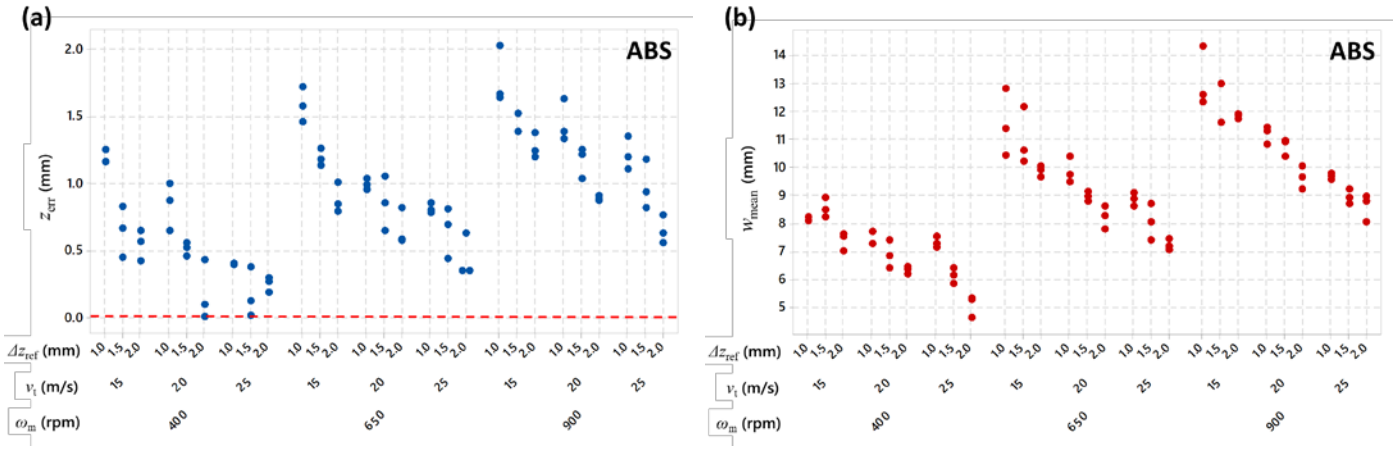

Fig. 5 *Experimental results for ABS: (a) individual value plot of mean height difference (Δz_{diff}); (b) individual value plot of mean width (w_{mean}).*

Fig. 3 shows three examples of PLA tracks that were deposited at different experimental conditions, while the individual value plots of Fig. 4 and Fig. 5 depict the experimental results in terms of mean height difference (Δz_{diff}) and mean width (w_{mean}) for PLA and ABS, respectively.

Regarding PLA, most of the process parameter combinations led to flattened tracks (for example, A and B in Fig. 3), which are favorable for building complex multi-layer objects since they can adhere successfully to each other. However, at two experimental conditions (ω_m = 400 rpm, v_t = 25 mm/s, Δz_{ref} = 2.0 mm and ω_m = 400 rpm, v_t = 25 mm/s, Δz_{ref} = 2.5 mm) the material was just laid on the heated table in the shape of undeformed filaments (for example, C in Fig. 3). Tracks with a rounded section are detrimental because adhesion issues could occur when overlapping them, therefore the aforementioned experimental conditions leading to such tracks correspond to unsuitable process parameter combinations for printing PLA. In case of ABS, flattened tracks were produced at all the experimental conditions.

A linear regression analysis with uncoded predictors was performed to point out the relationship between the three selected process parameters and the two responses describing the track geometry (that is, the height difference and the mean width) for both PLA and ABS. Tab. 3 summarizes the main results of the regression analysis, namely, the factor p-values, the estimated standard deviation, the coefficient of determination (R^2_{adj}) and the p-value of the lack-of-fit (LOF) test for each analyzed model. The results of Tab. 3 show how all factors and some interactions between them influence the responses. The estimated regression models of the two responses are expressed by the Equations (2) and (3) for PLA and the Equations (4) and (5) for ABS. For the sake of hierarchical completeness, some not significant factors are left in the model and the corresponding terms are in square brackets. The coefficient of determination (R^2_{adj}) high values and the high p-values of the lack of fit test demonstrate the adequacy of all the regression models [29].

Tab. 3 *Regression analysis results: factor p-values (α = 1%, bold: significant factors, italic: nearly significant factor), estimated standard deviations, R^2_{adj} and LOF p-values.*

		factor p-value								**estimated standard deviation (mm)**	R^2_{adj}	**LOF p-value**
		ω_m	v_t	Δz_{ref}	ω_m*v_t	ω_m*Δz_{ref}	v_t*Δz_{ref}	ω_m^2	v_t^2			
PLA	Δz_{diff}	**0.000**	*0.020*	0.128	*0.013*	*0.014*	- - -	- - -	- - -	0.1103	89.93%	0.632
	w_{mean}	**0.000**	**0.000**	**0.003**	**0.000**	**0.002**	**0.001**	**0.001**	**0.001**	0.2704	97.28%	0.144
ABS	Δz_{diff}	**0.000**	**0.000**	**0.000**	- - -	- - -	*0.011*	- - -	- - -	0.1422	89.46%	0.263
	w_{mean}	**0.000**	**0.006**	**0.000**	**0.000**	- - -	- - -	**0.000**	*0.015*	0.4822	94.32%	0.784

$$\Delta z_{diff\_PLA} = -0.107 + 0.0017 \cdot \omega_m + 0.0444 \cdot v_t \left[-0.236 \cdot \Delta z_{ref} \right] - 0.00004 \cdot \left(\omega_m \cdot v_t \right) - 0.01916 \cdot \left(v_t \cdot \Delta z_{ref} \right) \quad (2)$$

$$w_{mean\_PLA} = 8.10 + 0.0172 \cdot \omega_m - 0.580 \cdot v_t - 1.390 \cdot \Delta z_{ref} - 0.00021 \cdot \left(\omega_m \cdot v_t \right) - 0.0012 \cdot \left(\omega_m \cdot \Delta z_{ref} \right) + 0.0661 \cdot \left(v_t \cdot \Delta z_{ref} \right) + -0.000004 \cdot \left(\omega_m \right)^2 + 0.0088 \cdot \left(v_t \right)^2 \quad (3)$$

$$\Delta z_{diff\_ABS} = 2.587 + 0.00137 \cdot \omega_m - 0.0928 \cdot v_t - 1.000 \cdot \Delta z_{ref} \left[+0.02506 \cdot \left(v_t \cdot \Delta z_{ref} \right) \right] \quad (4)$$

$$w_{mean\_ABS} = 10.02 + 0.02163 \cdot \omega_m - 0.541 \cdot v_t - 1.478 \cdot \Delta z_{ref} - 0.000283 \cdot \left(\omega_m \cdot v_t \right) - 0.000007 \cdot \left(\omega_m \right)^2 \left[+0.01142 \cdot \left(v_t \right)^2 \right] \quad (5)$$

Except for the unsuitable experimental conditions regarding PLA (ω_m = 400 rpm, v_t = 25 mm/s, Δz_{ref} = 2.0 mm and ω_m = 400 rpm, v_t = 25 mm/s, Δz_{ref} = 2.5 mm), all the other process parameter combinations are likely to be used to print multi-layer objects. Depending on the selected target material, the most suitable set of process parameters can be found through the Equation (2) or (4) setting a null (or nearly null) height difference, which corresponds to an appropriate throughput given by the extruder motor rotational speed and the translation speed for the layer height set in the robot motion control. For example, if the objective is to achieve the highest productivity, high levels of extruder motor rotational speed and robot translation speed should be selected, then the Equation (2) or (4) is used to identify the suitable value of nominal layer height. Once the most suitable process parameter combination has been identified, the Equation (3) or (5) can be used to estimate the track mean width. Finally, the values of the track height and width resulting from this selection process are given as input to the slicing software that is used to generate the part program for complex objects.

4. Process parameters online adjustment

4.1. Online layer height control (OLHC)

When multi-layer objects are manufactured, the material is likely to shrink and the over/under-pressure between consecutive layers could cause structural deformation. Indeed, even maintaining constant the rotational speed of the extruder motor and the robot translation speed, the height variation of the deposited layer may be not negligible. Remarkably, an actual layer height that is too low or too high can determine deformations in the manufactured object (Fig. 6 and Fig. 7).

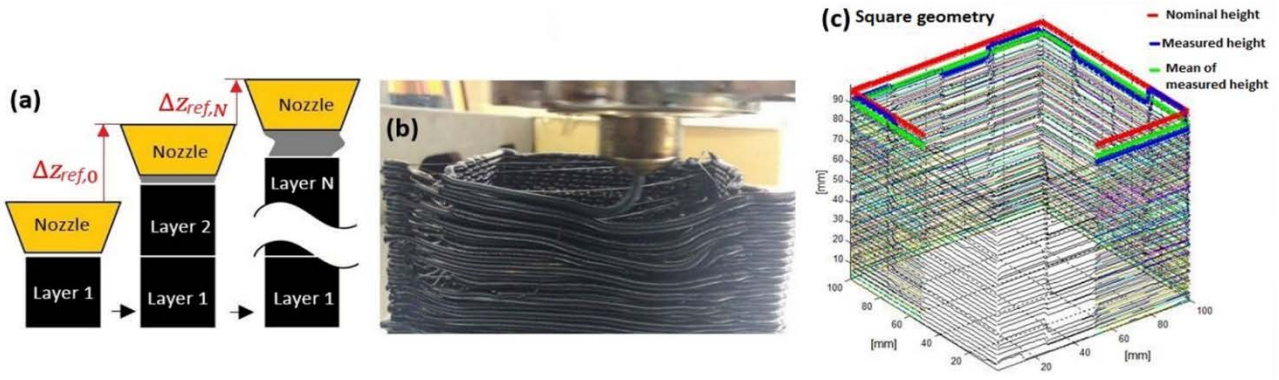

Fig. 6 *Robot height **above** the optimal range: (a) conceptual scheme; (b) deposition experiment; (c) deposition defect measured with laser sensor.*

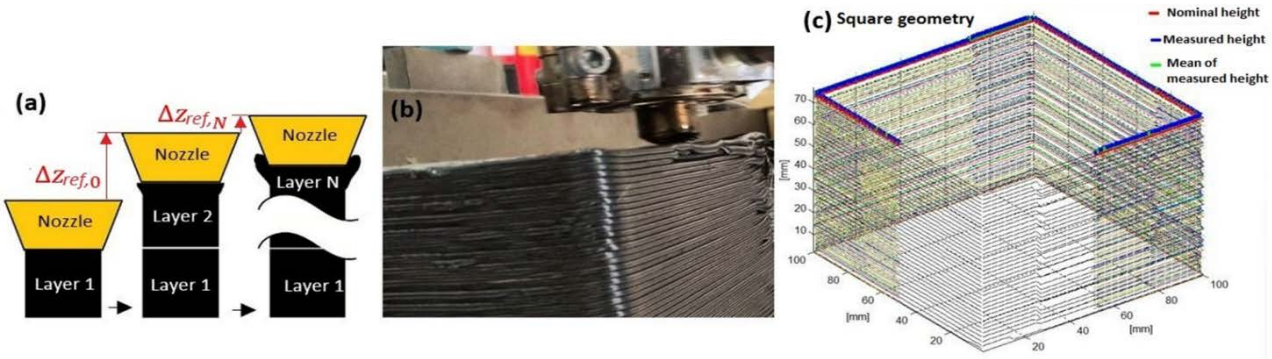

Fig. 7 *Robot height **under** the optimal range: (a) conceptual scheme; (b) deposition experiment; (c) deposition defect measured with laser sensor as error between nominal and measured layer height.*

An innovative strategy to cope with such problems, consisting in an Online Layer Height Control (OLHC) algorithm, has been presented by the authors in [30]. The suggested control strategy is based on laser sensor measurements to maintain the deviations in layer height and width within a tolerance range. Specifically, the algorithm overcomes the hypothesis that deposited layer height must be calculated offline. Indeed, the laser sensor (Fig. 2b) measures the distance between the deposited material and the extruder nozzle and the algorithm online modifies the layer height, in order to maintain an optimal overlapping (Fig. 8). In this way, it is possible to control the adhesion among consecutive layers and to reduce the deformations in the manufactured object.

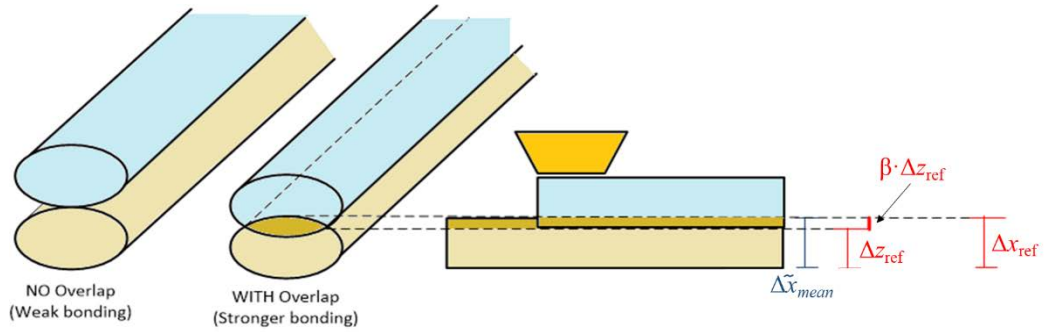

Fig. 8 *Scheme of the discrete control method: after the deposition of the underlying layer, $\Delta \tilde{x}_{mean}$ is measured with the laser sensor and compared with the reference layer height $\Delta z_{ref,0}$ increased by the overlap factor β.*

Mathematically, given a starting set of parameters ω_m, v_t, $\Delta z_{ref,0}$, the best height for the deposited polymeric material can be written as $\Delta x_{ref,0}$ that is higher than $\Delta z_{ref,0}$ in order to obtain the desired overlap β:

$$\Delta x_{ref,0} = (1+\beta)\Delta z_{ref,o} \quad ; \quad \beta \in [0.2 \div 0.3] \tag{6}$$

If the mean of the measured material height is denoted as $\Delta \tilde{x}_{mean,0}$, the error between the nominal material height and the measured one can be written as:

$$e_0 = \Delta \tilde{x}_{mean,0} - \Delta x_{ref,0} \tag{7}$$

Hereafter, a simple proportional control algorithm at the k[th] layer can be set to reduce the error, as shown in Equation (9):

$$e_k = \Delta\tilde{x}_{mean,k} - \Delta x_{ref,k} = \Delta\tilde{x}_{mean,k} - (1+\beta)\Delta z_{ref,o} \quad ; \quad \forall k = 0 \ldots N-1 \tag{8}$$

$$\Delta z_{ref,k+1} = \Delta z_{ref,k} + \lambda(e_k) = \Delta z_{ref,k} + \lambda\left(\Delta\tilde{x}_{mean,k} - (1+\beta)\Delta z_{ref,k}\right) \quad ; \quad \forall k = 0 \ldots N-1 \tag{9}$$

This implies that the robot trajectory is modified with the computed height $\Delta z_{ref,k+1}$, minimizing the error with a correct gain $\lambda < 1/(1+\beta)$ that is able to guarantee a proper convergence. Furthermore, in [30] it is shown that this control strategy leads to a convergence towards optimal process parameters also in the case that a complete process parameter tuning (Section 3) cannot be performed.

In order to show the effectiveness of the proposed adjustement method, two tests have been performed printing a square geometry using PLA. Initially, the commanded layer height has been set at an optimal value ($\Delta z_{ref,0}$ =2.2 mm) being in the centre of the operative range identified in Section 3 for PLA. This value guarantees a regular behavior and reduces the dimensional errors for many layers. Fig. 9a shows the improvements that can be achieved applying the layer height control loop when $\Delta z_{ref,0}$ is too high, such as in case of underlying material shrinkage (in the proposed example, $\Delta z_{ref,0}$ is set 15% higher than the optimal value). If the control algorithm is not used, the mean layer height error e_k (Equation (8)) increases. The material collapsing and creating curls or irregular rods cause an increase of the mean layer width error. Thanks the robot height adaptation algorithm (Equation (9)), the layer shape can be mantained under control and within a tolerance interval. Fig. 9b shows that similar improvements can be obtained if $\Delta z_{ref,0}$ is lower than the optimal value (in the reported experiment, $\Delta z_{ref,0}$ is set 15% lower than the optimal value). Similar improvements have been achieved also using ABS, which has a higher shrinkage ratio and, as a consequence, is subject to significant deformations of the artifact. In Fig. 10, a defect in the ABS object is shown, due to an excess of material caused by a layer height that is too small.

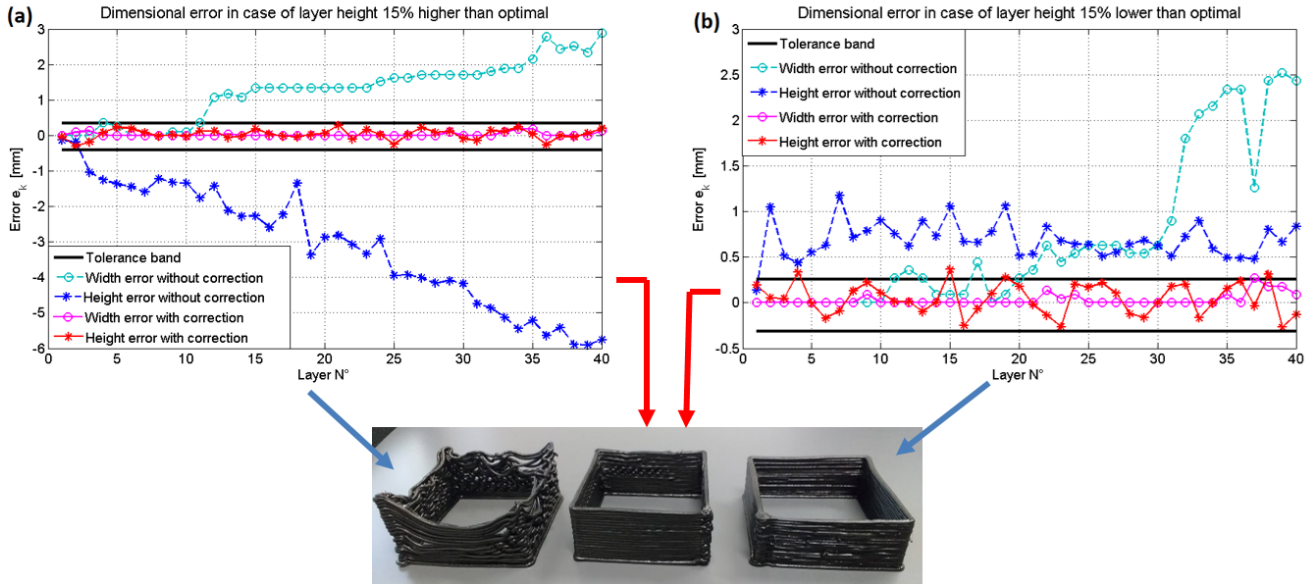

Fig. 9 *Measured dimensional errors (mean layer height error and mean layer width error) for each layer of a square geometry printed with PLA: (a) error caused by robot height 15% above the optimal range and its correction using the OLHC algorithm; (b) error caused by robot height 15% below the optimal range and its correction.*

Fig. 10 *Dimensional errors on a simple ABS object.*

The methodology can be applied to the deposition of both the contour and the infill of the parts. However, since the height modification is computed layer by layer, locally some step/gap between the segments of paths may occur. Indeed, when the path geometry is very different for the contour with respect to the infill, different shrinkage behaviors may occur. As matter of example, this issue may happen when the infill is very dense, but weakly connected to the contour.

4.2. Online re-slicing

Section 4.1 describes the method for the online control of the height of each deposited layer (OLHC). The drawback of this technique consists in the heuristic used to find the β parameters and this correction results in a final height of the printed object that is different from the desired height indicated in the CAD design. Indeed, the first slicing of the object is realized with an initial fixed guess for the layer height. As a consequence, when using the monitoring and correction of the layer height, an online communication between the robotic system and the computer running the slicing software is necessary. The robot controller

provides the new layer height to the computer and receives the new printing path where the object geometry has been sliced according to the corrected parameters. This re-slicing has to be performed each time that the total layer height correction due to the control loop is higher than a given threshold.

In this work one of the most recent algorithms available in literature [31] (Section 4.2.2) has been modified and customized (see Section 4.2.3) with a massive exploitation of parallel computing, thanks to the use of a GPU instead of CPU. Indeed, GPU architecture is appropriate especially for applications with relatively simple tasks repeated in large datasets. The short computational times that can been achieved in this way are particularly suitable for the online re-slicing.

4.2.1. Assumptions

The proposed approach relies on the following assumptions:

- The online re-slicing algorithm (ORA) has been implemented only for tessellated STL models, the so-called "direct slicing" algorithms that work directly on CAD-generated models are not taken into account in this work.
- The algorithm does not generate the "infill" path, but only the "perimeters". This means that this study does not consider optimization algorithms to fill the object geometry from a topological point of view.

4.2.2. First slicing

The GPU-based algorithm for parallel slicing presented in [31] has been implemented for the first slicing (which is performed offline, before the start of the printing process). Specifically, the methodology in [31] ((a) in Fig. 11) consists of two phases: (i) the preprocessing sort algorithm ((a.1) in Fig. 11 and Fig. 12) and (ii) the slice computation algorithm ((a.2) in Fig. 11 and Fig. 12), exploiting a heavy parallelized computation programmed with CUDA libraries. In the preprocessing sort phase, all the triangles that intersect with the same plane are stored in the same group (or bucket). Then, in the slice creation phase, for each triangle in a group and for each group, a thread is created to perform the "triangle-plane calculation" [32]. The threads are divided among the "blocks" and the "grids" of the GPU, considering the optimal GPU "block" dimension that can be determined with tools such as the CUDA Occupancy Calculator [31]. After performing the whole slicing step, all the obtained segments are processed with standard "contour construction" and "path creation" procedures ((b) and (c) in Fig. 11, respectively). The path is finally post-processed and translated into the ABB RAPID language to get the robot part-program.

4.2.3. Online Re-slicing Algorithm (ORA)

As described in [30], the robotized AM system measures each deposited layer and computes the new commanded robot height. If this new height exceeds a given threshold, the Online Re-slicing Algorithm (ORA) is applied as follows:

1) The ABB robot sends via TCP/IP the information about the new commanded layer height $\Delta z_{ref,k+1}$ and the actual height $z_{reslice}$ where the robot is placed when the re-slicing is ordered.
2) The program running on the computer receives this information and perform the slicing starting from $z_{reslice}$. This means that all the "slicing groups" that include only z-coordinates lower than $z_{reslice}$ should not be considered by the slicing algorithm, as

well as all the triangles whose vertices are entirely located under the $z_{reslice}$ coordinate. As a consequence, in this "slicing phase" ((a) in Fig. 11), the preprocessing sort algorithm ((a.1) in Fig. 11 and Fig. 12) and the slice computation algorithm ((a.2) in Fig. 11 and Fig. 12) are implemented.

3) Once the GPU-based slicing phase has been performed, the contour and the printing path are generated. Then the post-processor is activated to translate the path stored in memory array into the ABB RAPID language. Therefore, the module files containing the post-processed instructions are sent to the robot controller via FTP protocol and a signal via the Ethernet connection informs the robot controller to drop the old files and load the new ones.

4) The robot is now allowed to restart the printing process following the new instructions.

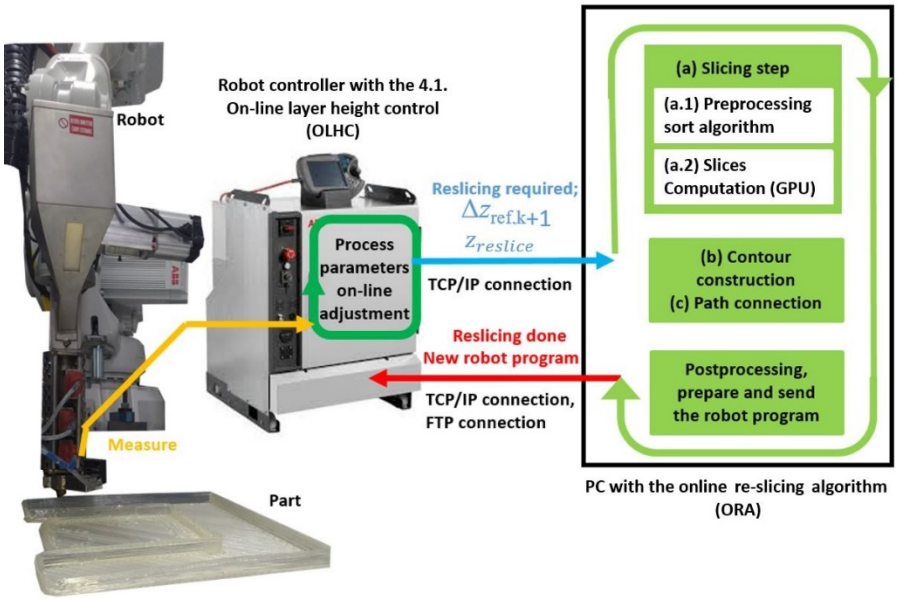

Fig. 11 *Overall scheme of the process parameters online adjustment and CAD file online re-slicing.*

Algorithm a.1: Preprocessing Sort

Input: *T* (Triangles vertices in the STL file whose vertices are < $z_{reslice}$)
Output: Bucket List *B*

```
B ← Create a list of buckets();
foreach triangle t in T do
    Find min and max z axis coordinate for t;
    Let Index_lowest be the index of the lowest bucket intersecting t;
    Index_lowest = (triangle_minz − z_reslice) / Δz_ref.k+1
    Index_highest = (triangle_maxz − z_reslice) / Δz_ref.k+1
    for i = Index_lowest to Index_highest − 1 do
        B[i].Add(t);
return B;
```

Algorithm a.2: Slices Computation

Input: Bucket List *B*
Output: Line Segments *S*

```
S ← Create a list of lines();
i = 0;
foreach bucket b in B do
    foreach triangle t in b do
        Line = calculate_intersection(); (see appendix A)
        S[i].Add(Line);
    i++;
return S;
```

Each basic calculation on a different thread of GPU

Fig. 12 *(a) algorithm for the pre-processing sort of the triangles to be printed at a height higher than $z_{reslice}$; (b) algorithm for the GPU-based slices computation as proposed in [26].*

5. Case study

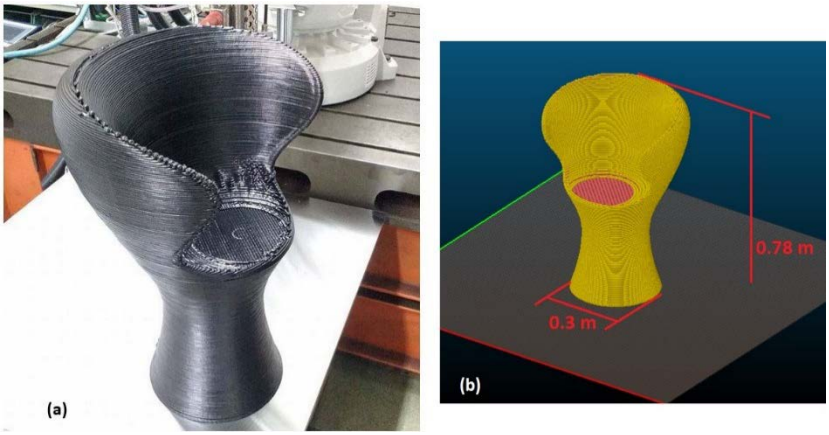

Fig. 13 *(a) final example of an object obtained with the described setup: chair made using PLA mixed with black colorant; (b) CAD file of the printed chair visualized using the Slic3r© software.*

As a representative case study, a piece of furniture has been manufactured in PLA using the setup described in Section 2. The extruder temperature range was 147 °C - 164°C, the heated bed temperature was 88°C and the following process parameters within the optimal range found in Section 3 were used: ω_m = 650 rpm, v_t = 25 mm/s, Δz_{ref} = 2.2 mm. In this case, the system has a deposition flow rate of about 1250 cm^3/h; the chair in Fig. 13a has been produced in about 6 hours.

To demonstrate the effectiveness of the proposed online re-slicing algorithm, the extruder head trajectory has been generated with two approaches: (i) based on a custom version of the open-source Slic3r© software [33], which can act as a CAD/CAM software for the considered system and generate a part program with the motion instructions for both the robot and the extruder; (ii) based on the CUDA-based slicer described in Section 4.2.3. Slic3r© does not take advantage of GPU and with the standard settings it uses two parallel threads to calculate the path. The computational time is measured only for the "slicing step" thanks to a "tic/toc" pair placed around the GPU-based algorithm or around the system call to the command line that Slic3r© generates to perform the slicing without the graphical interface.

Tab. 4 *Comparison of computational times for performing the slicing of the object in* ***Fig. 13****.*

Using Slic3r© [s]	Using CUDA-based slicer [s]
2.77	0.315

The selected object is modelled as a STL file with 35986 facets and has a total height of 780 mm, resulting in 354 layers with a first-guess layer height of 2.2 mm. The measured computational times are reported in Tab. 4. The results highlight that the time needed for the slicing is reduced by 9 times when using the CUDA-based slicer. The advantages of the GPU are clear and they are expected to be more relevant if the layer thickness is lower or the object is bigger (this means that it will be composed by more slices and, thus, that there will be more operations to parallelize).

The OLHC algorithm described in Section 4.1 has also been applied. Measurements with the laser sensor have been performed every 10 layers and the results showed that the selected process parameters were leading to a material accumulation. Consequently, the correction algorithm gradually increased the commanded robot height and the chair resulted to be 8.8 mm higher compared to the original design. This result points out how a constant shape of the deposited tracks and, therefore, a successful manufacturing of complex geometries are guaranteed using the layer height control algorithm, but the desired object height cannot be precisely achieved, if the re-slicing strategy is not adopted. In the analyzed case study, the height error has been removed thanks to the online re-slicing algorithm, which have been performed four times during the whole printing process.

6. Conclusions

In this study, a flexible AM platform for big plastic objects has been realized mounting an industrial screw-based extruder on an anthropomorphic robot. Suitable methods have been designed to overcome the limitations of the AM system and to avoid defects on the manufactured objects. The proposed approach consists of the following steps:

1) an experimental campaign designed according to DoE, aiming to set a suitable range of the most important process parameters (i.e. extruder motor rotational speed, robot translation speed, nominal layer height);
2) the OLHC algorithm, that is a closed loop control strategy able to correct the robot height and to guarantee a regular shape of each deposited layer);
3) the online re-slicing algorithm, being able to preserve the original size of the manufactured object, even though the closed loop control changes the layer height. The time required for the re-slicing step is maintained low thanks to an heavy exploitation of parallel computation on a NVIDIA GPU.

A representative case study demonstrated the effectiveness of the whole approach, achieving a deposition flow rate of 1250 cm^3/h.

Acknowledgements

The described setup has been developed in collaboration with Gimac International S.r.l., which manufactured the industrial extruder. Special thanks to Simone Maccagnan and Gianpiero Bianchi for the help. We also would like to thank ABB Robotics Italy for the support.

References

[1] I. Gibson, D. Rosen, B. Stucker, Additive manufacturing technologies: 3D printing, rapid prototyping and direct digital manufacturing, 2nd edition, Springer, New York, 2015.

[2] T. Wohlers, T. Caffrey, Wohlers report 2017: 3D printing and additive manufacturing state of the industry annual worldwide progress report, Wohlers Associates, 2017.

[3] N. Guo, M.C Leu, Additive manufacturing: technology, applications and research needs, Front. Mech. Eng. 8(3) (2013) 215-243. https://doi.org/10.1007/s11465-013-0248-8

[4] Gimac S.r.l., Microextruders. http://www.gimac.com/eng/datitecnici012.php (accessed 19 June 2018).

[5] S.S. Babu, L. Love, R. Dehoff, W. Peter, T.R. Watkins, S. Pannala, Additive manufacturing of materials: opportunities and challenges, MRS Bull. 40(12) (2015) 1154-1161. https://doi.org/10.1557/mrs.2015.234

[6] G. Q. Zhang, X. Li, R. Boca, J. Newkirk, B. Zhang, T. Fuhlbrigge, H. Feng, N. Hunt, Use of industrial robots in additive manufacturing - a survey and feasibility study, Conference ISR ROBOTIK, Berlin, 2014.

[7] BAAM (Big Area Additive Manufacturing). http://web.ornl.gov/sci/manufacturing/ (accessed 19 June 2018)

[8] Branch Technology. http://www.branch.technology/ (accessed 19 June 2018)

[9] Stratasys Robotic AM. http://blog.stratasys.com/2016/08/24/infinite-build-robotic-composite-3d-demonstrator/, 2016 (accessed 19 June 2018)

[10] DeltaWASP 3MT. http://www.wasproject.it/w/en/3d-printing/deltawasp-3-mt/ (accessed 19 June 2018)

[11] M. Faes, W. Abbeloos, F. Vogeler, H. Valkenaers, K. Coppens, E. Ferraris, Process monitoring of extrusion based 3D printing via laser scanning, PMI 2014 Conference Proceedings, 6 (2014) 63-67. https://doi.org/10.13140/2.1.5175.0081

[12] A.K. Sood, Study on parametric optimization of fused deposition modelling (FDM) process, PhD thesis, National Institute of Technology Rourkela, 2011.

[13] M. Montero, S. Roundy, D. Odell, S.H. Ahn, P.K. Wright, Material characterization of fused deposition modeling (FDM) by designed experiments, Proceedings of Rapid Prototyping and Manufacturing Conference, SME (2001) 1-21.

[14] R. Anitha, S. Arunachalam, P. Radhakrishnan, Critical parameters influencing the quality of prototypes in fused deposition modelling, J. Mater. Process. Technol. 118(1-3) (2001) 385-388. https://doi.org/10.1016/S0924-0136(01)00980-3

[15] Y. Zhang, K. Chou, A parametric study of part distortions in fused deposition modelling using three-dimensional finite element analysis, Proc. Inst. Mech. Eng. Part B-J. Eng. Manuf. 222(8) (2008) 959-968. https://doi.org/10.1243/09544054JEM990

[16] J. Mazumder, D. Dutta, N. Kikuchi, A. Ghosh, Closed loop direct metal deposition: art to part, Opt. Lasers Eng 34(4-6) (2000) 397-414. https://doi.org/10.1016/S0143-8166(00)00072-5

[17] R.B. Dinwiddie, L.J. Love, J.C. Rowe, Realtime process monitoring and temperature mapping of a 3D polymer printing process, SPIE Defense, Security, and Sensing. International Society for Optics and Photonics (2013) 1-9. https://doi.org/10.1117/12.1518454

[18] R.B. Dinwiddie, V. Kunc, J.M. Lindal, B. Post, R. Smith, L. Love, C. Duty, Infrared imaging of the polymer 3D-printing process, SPIE Sensing Technology + Applications. International Society for Optics and Photonics (2014) 1-12. https://doi.org/10.1117/12.2053425

[19] M. Faes, W. Abbeloos, F. Vogeler, H. Valkenaers, K. Coppens, E. Ferraris, Process monitoring of extrusion based 3D printing via laser scanning, PMI 2014 Conference Proceedings, 6 (2014) 63-67. https://doi.org/10.13140/2.1.5175.0081

[20] R. Minetto, N. Volpato, J. Stolfi, R.M. Gregori, M.V. Da Silva, An optimal algorithm for 3D triangle mesh slicing, Comput.-Aided Des. 92 (2017) 1-10. https://doi.org/10.1016/j.cad.2017.07.001

[21] P.M. Pandey, N.V. Reddy, S.G. Dhande, Slicing procedures in layered manufacturing: a review, Rapid Prototyping J. 9(5) (2003) 274–288. https://doi.org/10.1108/13552540310502185

[22] J. Xu, W. Hou, Y. Sun, Y.S. Lee, PLSP based layered contour generation from point cloud for additive manufacturing, Robot. Comput.-Integr. Manuf. 49 (2018): 1-12.

[23] D. Ding, Z. Pan, D. Cuiuri, H. Li, N. Larkin, S. Van Duin, Automatic multi-direction slicing algorithms for wire based additive manufacturing, Robot. Comput.-Integr. Manuf. 37 (2016): 139-150.

[24] J.S. Panchagnula, S. Simhambhatla, Manufacture of complex thin-walled metallic objects using weld-deposition based additive manufacturing, Robot. Comput.-Integr. Manuf. 49 (2018): 194-203.

[25] Y. Jin, Y. He, G. Fu, A. Zhang, J. Du, A non-retraction path planning approach for extrusion-based additive manufacturing, Robot. Comput.-Integr. Manuf. 48 (2017): 132-144.

[26] C. Kirschman, C. Jara-Almonte, A parallel slicing algorithm for solid freeform fabrication processes, Solid Freeform Fabrication Symposium (1992) 26–33.

[27] K. Tata, G. Fadel, A. Bagchi, N. Aziz, Efficient slicing for layered manufacturing, Rapid Prototyping J. 4 (1998) 151–167. https://doi.org/10.1108/13552549810239003

[28] NVIDIA, CUDA Compute unified device architecture programming guide (version 1.0). http://developer.download.nvidia.com/compute/cuda/1.0/NVIDIA_CUDA_Programming_Guide_1.0.pdf, 2007 (accessed 19 June 2018)

[29] D.C. Montgomery, Design and Analysis of Experiments, eighth ed., Wiley, New York, 2012.

[30] P. Magnoni, L. Rebaioli, I. Fassi, N. Pedrocchi, L. Molinari Tosatti, Robotic AM system for plastic materials: tuning and online adjustment of process parameters, Proc. Manuf. 11 (2017) 346-354. https://doi.org/10.1016/j.promfg.2017.07.117

[31] X. Zhang, G. Xiong, Z. Shen, Y. Zhao, C. Guo, X. Dong, A GPU-based parallel slicer for 3D printing. Conference on Automation Science and Engineering (CASE) (2017). https://doi.org/10.1109/COASE.2017.8256075

[32] H.S.M. Coxeter, Planes and Hyperplanes, in: H.S.M. Coxeter, Introduction to geometry, second ed., Cambridge University Press, 1989.

[33] Slic3r open source software. http://slic3r.org/ (accessed 19 June 2018).